THE AEOLIAN ENVIRONMENT OF THE LANDING SITE FOR THE EXOMARS ROSALIND FRANKLIN ROVER IN OXIA PLANUM, MARS. E.A. Favaro[1], M.R. Balme[1], J. Davis[2], P.M Grindrod[2], P. Fawdon[1], A.M. Barrett[1], S.R. Lewis[1], School of Physical Sciences, Open University, Walton Hall, Milton Keynes MK7 6AA, UK (elena.favaro@open.ac.uk), Department of Earth Sciences, Natural History Museum, London, UK.

Introduction: The European Space Agency's ExoMars *Rosalind Franklin* Rover (ERFR) is due to land at Oxia Planum (OP) in 2023 [1]. The goal of ERFR is to search for signs of life on Mars [2] through the identification and subsequent analyses of target rocks with the highest biomarker preservation potential. To do this, ERFR must be able to identify and safely maneuver to potential sample sites. Therefore, comprehensively characterizing the aeolian landscape of the landing site prior to the start of operations is of utmost importance [3].

The motivation for this work is to characterize the wind regime and erosional history of OP using a combination of machine learning and observational (manual mapping and change detection) techniques to analyze the migration, morphometrics, distribution, and orientation of transverse aeolian ridges (TARs), periodic bedrock ridges (PBRs), dust devils, and windstreaks in and around the 1-sigma landing ellipses (Fig. 1). In the absence of in-situ near surface wind speed and direction data, we used Global Circulation Model (GCM) near surface winds derived from several contemporary re-analyses of spacecraft thermal and dust opacity data [4] to obtain the best possible understanding of the current wind regime at OP.

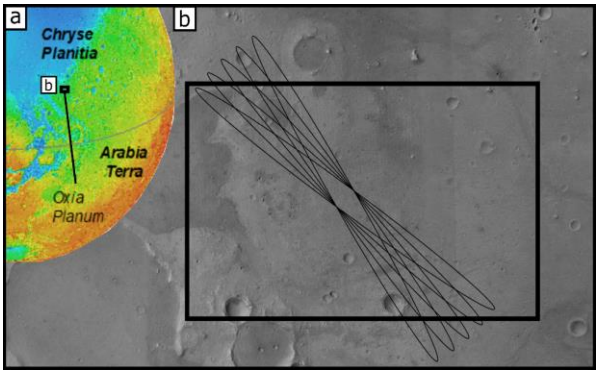

Figure 1. (a) Regional context for (b) Oxia Planum. The study site and 1-sigma landing ellipses are outlined. Background image is HRSC basemap. HiRISE, CaSSIS, CTX, HRSC footprints for observations can be found in [3].

Methods: *Machine Learning:* the NOAH-H (NOvelty and Anomaly Hunter – HiRISE) [5] machine learning system is a deep learning neural network developed to classify terrain types within a HiRISE [6] image into ontological classes. These include different TAR-like bedform morphologies, (divided into 'discontinuous' and 'continuous' TARs), and bedrock classes which can be used to identify PBR morphologies. *Discontinuous TARs* denote TARs that are separated from one another by areas of non-aeolian material; *continuous TARs* describe patches of TARs which merge downwind into one another, or which are separated only by areas of the same aeolian material which forms the TARs [3]. *Manual Mapping:* Directionality and distribution of TARs and PBRs was measured by digitizing crestlines from HiRISE image data in a GIS in a 640 km^2 area of OP (Fig. 1). The area was gridded into 160 4 km^2 quadrants, with every second quadrant analyzed. *Change Detection:* Orthorectified and coregistered repeat HiRISE imaging of a TAR field close to the study area was searched for ongoing movement over five martian years. Active dust devils were identified within the study area, and their speed and directionality mapped using HRSC [7] and CaSSIS [8] images. Change detection between consecutive CTX [6] images was used to analyze any alteration in dust devil tracks and/or windstreaks on the surface to gain a better understanding of present-day wind conditions [3].

Observations and Discussion: We digitized and measured the along-crestline lengths and orientations of 7989 continuous TARs, 2764 discontinuous TARs, and 457 PBRs. Along-crestline length and orientations are reported in Table 1 and displayed in Fig. 2, respectively. TARs are found extensively across OP; within topographic lows, in craters, and on undulating plains. Where TARs are large enough to distinguish tonal variations across them, we find that the flank northwest of the crest line is almost always of lower albedo than the southeastern flank [3]. We used this variation and the established grainsize-albedo relationship of stoss and lee slopes seen in terrestrial megaripples [10] to interpret stoss and lee slopes of OP TARs. Accordingly, winds blowing from the NW-NNW to the SE-SSE were responsible for present-day TAR orientation (Fig. 2). We did not note any TAR migration in OP in repeat HiRISE images.

PBRs occur across OP, but most frequently in low relief areas of the south-central region. Craters, topographic lows, and fractures intersect PBR crestlines, exemplifying the cohesive nature of their substrate [3]. PBRs develop perpendicular to the

direction of dominant wind [8-9], signaling that the winds responsible for abrasion of PBRs at Oxia Planum would need to originate between N-NNE or S-SSW. Until indicators of stoss/lee patterns can be observed by ERFR, there is 180° ambiguity in our analysis.

Table 1. the average orientation and the along-crestline length (L) characteristics for TARs and PBRs.

	n	Crestline Length Orientation[1]	L_{min} (m)	L_{max} (m)
C. TARs	7989	60°/240°	1.1	57.9
D. TARs	2764	61°/241°	1.1	556.0
PBRs	457	98°/278°	4.1	601.5

[1] *Accounting for 180° ambiguity*

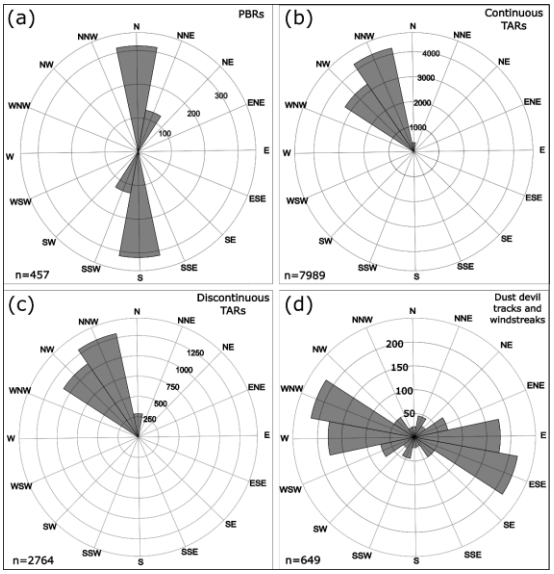

Figure 2. Directional roses (direction from which winds are inferred to blow) for the formative winds responsible for associated features. Values on the concentric circles denote frequency of occurrence.

Dust Devils and Windstreaks: We identified six active dust devils that did not have multiple imaging and 649 dust devil tracks and/or windstreaks, that had appeared between the CTX image pair taken 50 Earth days apart. These surface features had lengths from 0.13 to 10.1 km and are oriented predominantly in a WNW-ESE direction (with 180° ambiguity), although there is a smaller secondary direction distribution of NNE-SSW (Fig 2). This direction agrees with the direction of the two active dust devils. The density of dust devils and dust devil tracks and/or windstreaks reached densities of up to 16 km^{-2} in some places to the north of the study area, with an overall mean density of ~2.5 km^{-2} [3]. *Climate Modeling:* We compared the GCM winds from the reanalysis at 1.5 m above the surface at OP for MY 25 (global dust event year), 26, and 33 (no dust events); MY 26 and MY33 use assimilation of data from two different instruments and spacecraft. GCM predictions for all three years show variable directionality and the large-scale winds modelled explicitly in the GCM did not exceed 20 ms^{-1}[3], with winds often less than 10 ms^{-1}. The strongest winds originated from the north or south-east. An analysis of seasonality (at Ls=0/360, 90, 180, 270) reveal similar seasonal patterns typified by variable wind speed and direction that could not account for the orientation of aeolian features [3].

Conclusions: Based on analyses and interpretation of the action of the wind recorded in TARs, PBRs, dust devils, and wind streaks [3], we conclude that *(i)* the oldest wind direction is recorded in the rock record through the orientation of PBRs, which required either N-NNE or S-SSE blowing winds (accounting for 180° ambiguity) to develop; *(ii)* a second wind epoch is preserved in TARs. Irrespective of size, TARs display a consistent azimuthal orientation, necessitating winds blowing from the NW-NNW towards the SE-SSE to form; (*iii)* dust devils and windstreaks suggest the contemporary wind regime includes winds blowing from the WNW towards the ESE and infrequently from the NNE to the SSW. In addition, dust can be transported locally by dust devil action*; (iv)* TARs show no indication of movement in repeat HiRISE images, suggesting contemporary winds lack the necessary strength to mobilize TAR-forming materials.

Overall, we found evidence of a dynamic wind regime, active on multiple timescales, at OP. *In situ* data from ERFR will further refine our understanding of the aeolian environment of the landing site when it lands in 2023.

Acknowledgments: We gratefully acknowledge support from the UK Space Agency, UK Science and Technology Facilities Council, and the European Space Agency. The standard data products used here are available from the NASA PDS (https://pds.jpl.nasa.gov/).

References: [1] Vago et al. (2018), *ESA.* [2] Vago et al. (2017) *Astrobiology, 17,* (6-7). [3] Favaro et al. (2021 – In Press), *JGR.* [4] Holmes et al. (2020), *Planet Space Sci,* 104962. [5] Balme et al. (2019), *LPSC (2132).* [6] Malin et al. (2007), *JGR, 11(E5).* [7] Jaumann et al. (2007), *Planet Space Sci, 55,* 7-8. [8] Vago et al. (2015), *Sol. Syst. Res., 49(7).* [9] Montgomery et al. (2012), *JGR: Planets,* 117(E3). [10] Hugenholtz et al. (2015), *Aeolian Res., 18.* [11] Favaro et al. (2020), *Icarus, 346.*